

See discussions, stats, and author profiles for this publication at: <https://www.researchgate.net/publication/231390073>

Enhanced Mass Transfer of CO₂ into Water: Experiment and Modeling

ARTICLE in JOURNAL OF INDUSTRIAL AND ENGINEERING CHEMISTRY · JUNE 2009

Impact Factor: 3.51 · DOI: 10.1021/ie801521u

CITATIONS

39

READS

82

3 AUTHORS, INCLUDING:



R. Farajzadeh

Delft University of Technology

72 PUBLICATIONS 644 CITATIONS

SEE PROFILE



P. L. J. Zitha

Delft University of Technology

134 PUBLICATIONS 997 CITATIONS

SEE PROFILE

GENERAL RESEARCH

Enhanced Mass Transfer of CO₂ into Water: Experiment and Modeling

R. Farajzadeh,* P. L. J. Zitha, and J. Bruining

Department of Geotechnology, Delft University of Technology, Stevinweg 1, 2628 CN Delft, The Netherlands

Concern over global warming has increased interest in quantification of the dissolution of CO₂ in (sub-) surface water. The mechanisms of the mass transfer of CO₂ in aquifers and of transfer to surface water have many common features. The advantage of experiments using bulk water is that the underlying assumptions to the quantify mass-transfer rate can be validated. Dissolution of CO₂ into water (or oil) increases the density of the liquid phase. This density change destabilizes the interface and enhances the transfer rate across the interface by natural convection. This paper describes a series of experiments performed in a cylindrical PVT-cell at a pressure range of $p_i = 10\text{--}50$ bar, where a fixed volume of CO₂ gas was brought into contact with a column of distilled water. The transfer rate is inferred by following the gas pressure history. The results show that the mass-transfer rate across the interface is much faster than that predicted by Fickian diffusion and increases with increasing initial gas pressure. The theoretical interpretation of the observed effects is based on diffusion and natural convection phenomena. The CO₂ concentration at the interface is estimated from the gas pressure using Henry's solubility law, in which the coefficient varies with both pressure and temperature. Good agreement between the experiments and the theoretical results has been obtained.

1. Introduction

Carbon dioxide (CO₂) is one of the major greenhouse gases blamed for causing global warming.¹ To reduce the concentration of CO₂ in the atmosphere, geological storage of CO₂ is considered.^{2–4} When CO₂ is injected into an aquifer, the competition between viscous, capillary, and buoyancy forces determines the flow pattern. Eventually, due to buoyancy forces CO₂ will migrate upward and be trapped under the cap rock due to capillary forces. In this case an interface between a CO₂-rich phase and brine exists. Subsequently, CO₂ starts to dissolve into water by molecular diffusion when it is in contact with the brine. The dissolution of CO₂ increases the density of brine.⁵ This density increase together with temperature fluctuations in the aquifer (which may be only partially compensated by pressure gradients⁶) destabilize the CO₂–brine interface and accelerate the transfer rate of CO₂ into the brine by natural convection.^{5–10} The occurrence of natural convection significantly increases the total storage rate in the aquifer since convection currents bring the fresh brine to the top. Hence, the quantification of CO₂ dissolution in water and understanding the transport mechanisms are crucial in predicting the potential and long-term behavior of CO₂ in aquifers.

Unfortunately there are only a few experimental data in the literature, involving mass transfer between water and CO₂ under elevated pressures. Weir et al.¹¹ were the first to point out the importance of natural convection for sequestration of CO₂. Yang and Gu⁸ performed experiments in bulk where a column of CO₂ at high pressure was in contact with water. The procedure was similar to the established approach in which the changes in gas pressure relate the gas to the transfer rate.^{12–15} A modified diffusion equation with an effective diffusivity was used to describe the mass-transfer process of CO₂ into the brine. Good agreement between the experiments and the model was observed

by choosing effective diffusion coefficients 2 orders of magnitude larger than the molecular diffusivity of CO₂ into water. However, the authors pointed out that the accurate modeling of the experiments should consider natural convection effects. Farajzadeh et al.^{9,10} reported experimental results for the same system, in a slightly different geometry, showing initially enhanced mass transfer followed by a classical diffusion behavior in long times. A physical model based on Fick's second law and Henry's law was used to interpret the experimental data. It was found that the mass-transfer process cannot be modeled with a modified Fick's second law with a single effective diffusion coefficient for the CO₂–water system at high pressures. Nevertheless, the initial stages and later stages of the experiments can be modeled individually with the described model. Arendt et al.¹⁶ applied a Schlieren method and a three-mode magnetic suspension balance connected to an optical cell to analyze the mass transfer of the CO₂–water system up to 360 bar. Good agreement between their model (linear superposition of *free convection* and Marangoni convection) and the experiment was obtained. The addition of surfactant suppressed the Marangoni convection in their experiments, while in the experiments of ref 9, addition of surfactant did not have a significant effect on the transfer rate of CO₂. A similar mass-transfer enhancement was observed for the mass transfer between a gaseous CO₂-rich phase with two hydrocarbons (*n*-decane and *n*-hexadecane)^{9,10} due to the fact that CO₂ increases the hydrocarbon density.¹⁷ The effect becomes less significant with increasing oil viscosity. This has implications for oil recovery.

Indeed in geological storage of CO₂ the early time behavior is governed by diffusion before the onset of the natural convection.^{7,18,19} The critical time for onset of convection is a strong function of reservoir properties and in particular its permeability, which are lumped into the Rayleigh number in numerical simulations. Vella and Huppert²⁰ show that, for the Sleipner field, in which around 10⁹ kg of CO₂ is injected to a 200 m thick layer each year, with the typical measured values

* To whom correspondence should be addressed. E-mail: r.farajzadeh@tudelft.nl. Tel.: +31 (0)15 278 7961. Fax: +31 (0)15 278 1189.

for the porosity ($\varphi = 0.31$) and permeability of $0.7 \leq k \leq 5$ darcy the onset of convection may vary between a few days and 14.2 years. This suggests that the effect of gravity instabilities (convection) is indeed important in the field. Similar to the experiments with the *clear fluid*, natural convection effects in a saturated porous media also die out with time and eventually stop as more CO_2 is dissolved in brine (the driving force for convection decreases). This is one of the most important findings of our experiments, which is confirmed with the recent experiments conducted in porous media saturated with water²¹ and shown by simulation results.⁷ It should be noted that, in bulk experiments, the critical time for the onset of convection is very small.

The theoretical description of temperature-driven natural convection flow uses the Navier–Stokes equation and can be found in classical books on fluid mechanics.^{22,23} Several numerical approaches have been proposed to solve the governing Navier–Stokes and continuity equations. Guçeri and Farouk²⁴ derived a numerical model for steady-state natural (turbulent) convection in various geometries. By the symmetry of the geometries considered, they can use the stream function–vorticity approach. From the mathematical point of view these geometries allow a 2D description. Patankar²⁵ proposed a semi-implicit numerical method, which can also be used to (nonsteady) 3D problems. Bairi²⁶ used Patankar’s method to study the transient natural convection in a 2D vertical cylinder. Increasingly, the finite element method (FEM), which was originally developed for solid mechanics calculations, is being applied in this area. This method facilitates the modeling of the problem in complex geometries with irregularities.^{27–29} Moreover, nonuniform meshes can easily be used in this method which allow for the resolution of flow details in the regions of interest.

The purpose of this paper is 2-fold. The first objective is to demonstrate the importance of natural convection for storage of CO_2 in aquifers and to add experimental data to the currently small database in the literature. The second objective is to develop a model that can fully describe the experiments without having to introduce (semi-)empirical parameters, in spite of disregarding surface tension gradient and temperature effects. It turns out that this is possible by considering density-driven natural convection phenomenon. Therefore, this paper focuses on describing the phenomena, both experimentally and numerically, when a CO_2 -rich gaseous phase is on top of a water layer. Section 2 describes the geometry of the system and the physical model to study the natural convection in a vertical cylinder. Section 3 explains the experimental setup, i.e., a vertical cylindrical PVT cell and the experimental procedures. Section 4 presents the experimental results and compares it with the numerical computations. Finally we draw the main conclusions of this study.

2. Theoretical Model

2.1. Formulation. There can only be mechanical equilibrium in a fluid in a gravitational field if the concentration of CO_2 inside the liquid only varies in the vertical coordinate, i.e., $c = c(z)$. However if the concentration gradient exceeds a certain value mechanical equilibrium in the fluid will be impossible.²³ The instability will initiate a convection current. This process will develop into natural convection throughout the entire fluid, and the concentration becomes dependent on the radial coordinate as well. The driving force for natural convection is due to the fact that dissolution of CO_2 into water causes a density increase. Consequently fresh (no- CO_2 -containing) water moves to the interface and CO_2 -containing water moves downward,

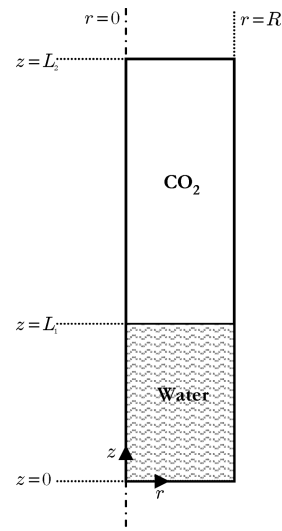


Figure 1. Schematic outlay of the process: The total length of the tube is L , the height of water is L_1 . There is no gas flowing out at the end of the tube. The gas–liquid interface is fixed. The liquid concentration at the interface is related to the gas pressure through Henry’s law and changes with time.

accelerating the diffusion process, and hence the mass-transfer rate. The mixing of the water finally leads to a constant CO_2 concentration in the water.

We try to formulate such motions inside the water when it is brought into contact with a CO_2 -rich gaseous phase in the geometry depicted in Figure 1. The cylindrical vessel with radius R consists of an upper column filled with gaseous CO_2 and a lower column filled with a stagnant water layer. We disregard both water evaporation (the contribution of water vapor to the gas pressure is 4.25 kPa at $T = 30^\circ\text{C}$, which is negligible compared to the experimental pressure drop³⁰) and water swelling due to CO_2 dissolution. Consequently we assume that the boundary remains fixed. This assumption arises from the fact that the volume change of the CO_2 –water binary mixture is very small at the range of our experimental pressures.³¹ It is assumed that capillary effects are absent, and therefore the interface is flat. The gas transfer at the upper part of the cell (gas phase) is very fast and therefore can be adequately described by Fick’s law with a high constant diffusion coefficient. CO_2 will be removed at the CO_2 –water interface. This decreases the concentration of CO_2 at the interface and increases the concentration of water. However, water concentration cannot deviate too far from equilibrium, as otherwise water will condense. Consequently, even with slow diffusion rates (of the order of $10^{-5} P_{\text{atm}}/P_{\text{exp}}$ m²/s) the concentration of CO_2 will not significantly deviate from its equilibrium value at the time scale of the experiment. The CO_2 concentration at the liquid surface is related to the gas pressure by assuming instantaneous thermodynamic equilibrium at the interface by applying Henry’s law. The characteristic time for conversion of $\text{CO}_2 + \text{H}_2\text{O} \rightarrow \text{H}_2\text{CO}_3$ is $1/0.039 - 25$ s, which is much smaller than the experimental times. Moreover, only a very small amount of CO_2 is converted to H_2CO_3 . The dissociation into HCO_3^- and CO_3^{2-} is negligible, and therefore the rates of their formation can be ignored. We assert that the transfer of gas through the CO_2 –water interface can be described as an unsteady-state diffusion process, i.e., by Fick’s law.

The conservation laws for the two components (CO_2 and water) and momentum in the liquid are the governing equations to describe the diffusion and natural convection; the analogy between mass and heat transfer allows us to use the equations

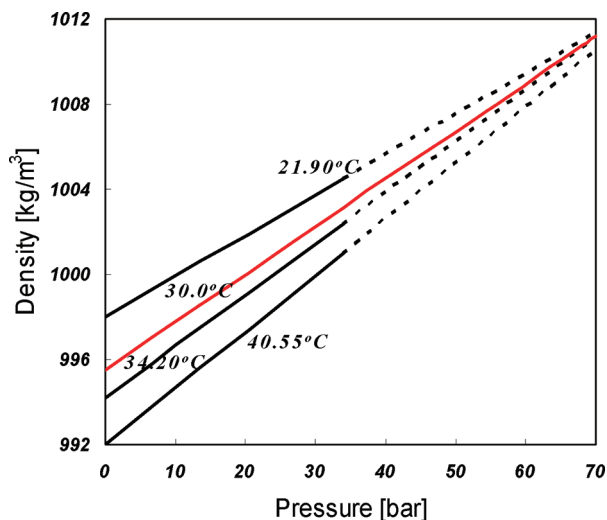


Figure 2. Density of water as a function CO₂ concentration (equilibrium pressure). The dashed lines are extrapolated from the solid lines reproduced from the data in ref 5.

in refs 22–24. Only a laminar regime is expected, as the Rayleigh number is of the order of 10⁶. The density difference is the driving force for natural convection, and consequently the density cannot be considered constant. However, we use the Boussinesq approximation, which considers density variations only when they contribute directly to the fluid motion. Moreover, we assume that there is a linear relationship between density change and concentration

$$\Delta\rho = \beta_c \rho_l \Delta c \quad (1)$$

Symbols are defined at the end of the paper. The characteristic behavior of the density of a CO₂–water solution on pressure and temperature can be found in ref 5. For the pressures and temperatures of interest the data are presented in Figure 2. The time dependent governing equations for a 2D diffusion and natural convection system can be written in radial coordinates (see Figure 1 for a schematic of the setup and the area of interest), as described below.

2.2. Governing Equations. 2.2.1. Liquid Phase. (a) Continuity Equation.

$$\text{div } \mathbf{v} = 0 \quad (2)$$

(b) Conservation of Momentum.

$$\frac{\partial \mathbf{v}}{\partial t} + (\mathbf{v} \cdot \text{grad}) \mathbf{v} = -\frac{1}{\rho} \text{grad } p + \nu \Delta \mathbf{v} - \beta_c \mathbf{g} \Delta c \quad (3)$$

(c) Concentration Equation.

$$\frac{\partial c}{\partial t} + \mathbf{v} \cdot \text{grad } c = D \Delta c \quad (4)$$

2.2.2. Gas Phase.

$$\frac{\partial c_g}{\partial t} = D_g \Delta c_g \quad (5)$$

One important dimensionless number in fluid dynamics is the Rayleigh number, which is dependent on the fluid properties and geometry of the system (characteristic length of the system) with the following relation

$$Ra = \frac{\beta_c g \Delta c R^3}{\nu D} = \frac{\Delta \rho g R^3}{\rho_l \nu D} \quad (6)$$

where we use eq 1 to replace β_c . Equation 6 states that the magnitude of the Rayleigh number depends on the geometry of the experimental setup, in this case the radius of the tube, and properties of the fluid. These properties include the diffusion coefficient of gas into water, the viscosity of the water, and its density change due to gas dissolution. As mentioned before in our case this density change is a strong function of the CO₂ concentration, i.e., the initial pressure of the CO₂. This means that a high Rayleigh number is due to a large radius of the tube or a high initial pressure or the combination of both parameters.

2.3. Boundary and Initial Conditions. 2.3.1. Liquid Phase. Initially the liquid is at rest and there is no CO₂ dissolved in the water; i.e.,

$$v = c = 0 \quad \text{at } t = 0 \quad (7)$$

The boundary conditions of the problem are

$$\begin{aligned} \partial_r c &= 0 \quad \text{at } r = 0 \\ v &= 0, \quad \partial_r c = 0 \quad \text{at } r = R \\ v &= 0, \quad \partial_z c = 0 \quad \text{at } z = 0 \\ c &= p_g/k_H = (Z_g R_B T/k_H) c_g \quad \text{at } z = L_1 \end{aligned} \quad (8)$$

2.3.2. Gas Phase. Initially the gas part is filled with gas at pressure p_i , and therefore the molar gas concentration reads,

$$c_g(x, t = 0) = \frac{p_i}{Z_g R_B T} \quad (9)$$

The boundary conditions are

$$\begin{aligned} \partial_r c_g &= 0 \quad \text{at } r = 0 \\ \partial_r c_g &= 0 \quad \text{at } r = R \\ J_z &= -D \partial_z c_g \quad \text{at } z = L_1 \\ \partial_z c_g &= 0 \quad \text{at } z = L_2 \end{aligned} \quad (10)$$

2.4. Henry's Law (CO₂ Solubility) at the Interface. The solubility of CO₂ in water can be expressed by Henry's law as

$$x_{\text{CO}_2(\text{aq})} = \frac{f_{\text{CO}_2(P,T)} \gamma_y}{k_H^*(P,T) \gamma_{\text{CO}_2(\text{aq})}} \quad (11)$$

where x_{CO_2} and y are the mole fractions of CO₂ in liquid and gas phases, respectively; k_H^* is Henry's constant (Pa) that is dependent on pressure and temperature; γ_{CO_2} is the asymmetric (Henry's law) activity coefficient of aqueous CO₂ such that $\gamma_{\text{CO}_2(\text{aq})} \rightarrow 1$ as $x_{\text{CO}_2(\text{aq})} \rightarrow 0$, γ_y is the symmetric (Raoult's law) activity coefficient of CO₂ in the nonaqueous phase such that $\gamma_y \rightarrow 1$ as $y \rightarrow 1$ and f_{CO_2} is the fugacity of pure CO₂ at specified P – T conditions. Henry's coefficient, k_H^* , can be calculated from the virial-like equation of state of Akinfiev and Diamond³²

$$\ln(k_H^*) = (1 - \xi) \ln f_w + \xi \ln \left(\frac{R_B T}{M_w} \rho_w \right) + 2 \rho_w \left[a + b \left(\frac{1000}{T} \right)^{0.5} \right] \quad (12)$$

Diamond and Akinfiev³³ developed a thermodynamic model that reproduces 362 published experimental solubility data with a precision of better than 2% over the entire P – T – x considered. We used their model to calculate Henry's coefficient (the model is available as a computer code at www.geo.unibe.ch/diamond). The dependency of Henry's coefficient, k_H ((Pa/mol)/m³), on

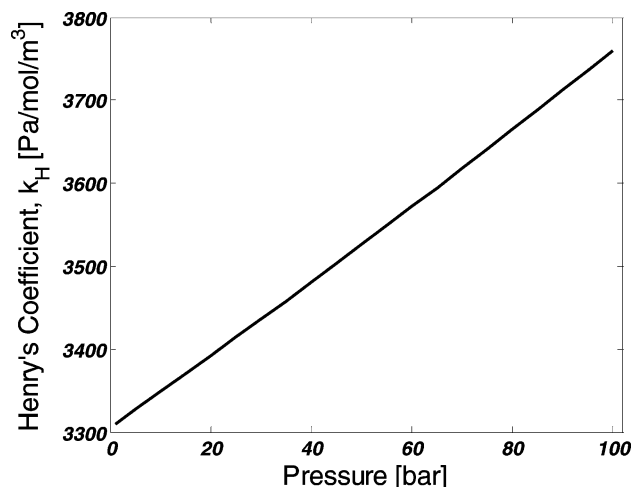


Figure 3. Henry's coefficient, k_H , as a function of pressure calculated using eq 12 at a constant temperature of $T = 30\text{ }^{\circ}\text{C}$.

pressure at a constant experimental temperature of $T = 30\text{ }^{\circ}\text{C}$ is shown in Figure 3. It is obvious that Henry's coefficient varies slightly with pressure at a constant temperature.

2.5. Numerical Scheme and Solution Procedure. The finite volume method (FVM) was first used to solve the model equations numerically. The validity of the model was confirmed by comparing to benchmark solutions. This model was used to validate the finite element method (FEM) in COMSOL Multiphysics, which is a software package that can solve various coupled engineering and physics problems, e.g., here a combination of Navier–Stokes, convection–diffusion, and diffusion equations in the geometry depicted in Figure 1. The advantage of FEM is that local grid refinement is easier and the simulation times are much smaller than FVM, especially when the Rayleigh values are large.

3. Experimental Section

3.1. Materials. The gas used to carry out the experiments was 99.98% pure carbon dioxide. CO_2 is highly soluble in water.³⁴ The diffusion coefficient of CO_2 in water is $D = (1.97 \pm 0.10) \times 10^{-9}\text{ m}^2/\text{s}$.³⁵ Nitrogen (N_2) was used to detect possible leakages in the setup. Water with $\text{pH} = 6.8 \pm 0.1$ was used in the experiments.

3.2. Setup and Procedure. Figure 4 shows the schematic of the experimental setup. It consists of two stainless steel vessels, the measurement vessel with an inner diameter of $D_1 = 30\text{ mm}$ and the gas storage vessel with an inner diameter of $D_2 = 40\text{ mm}$. The length of both vessels is 10 cm. The vessels are sealed and kept at a constant temperature of $T = 30 \pm 0.1\text{ }^{\circ}\text{C}$ in an oven. The characteristic time at which temperature equilibrates ($\sim 1500\text{ s}$) has been determined by numerical simulation, where the vessel was subjected to conductive and radiation heat loss. To ensure that the vessels remain in a fixed position, they were attached to a board. Before starting the measurements a leakage test was performed with nitrogen. A valve at the bottom of the measurement cell was used to fill the vessel with double distilled water up to the desired height ($L_1 = 43\text{ mm}$) using a pump with a known flow rate. A waiting time of approximately 1 h was then respected, in order to let the liquid come into thermal equilibrium with the oven. CO_2 was slowly injected into the measurement vessel from the storage vessel. The gas pressure was measured with two calibrated pressure gauges, which are connected to the top of the vessels. When the CO_2 pressure reached the desired value,

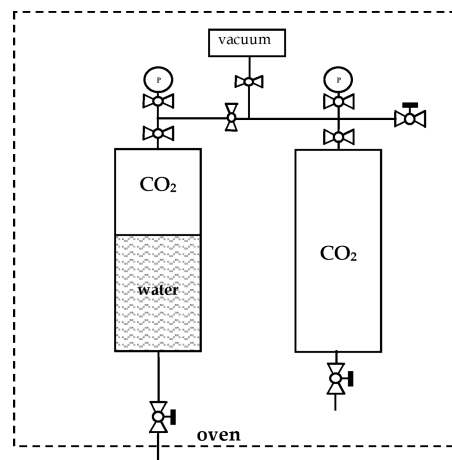


Figure 4. Schematic of the setup. The setup consists of two steel vessels, a storage vessel (right) and a measurement vessel (left). The gas at pressure p_i is injected from the right vessel to the left vessel. Mass transfer occurs through the interface in the left vessel. The setup is held in an oven at a constant temperature. The pressure of the gas at the top part is monitored by a pressure transducer.

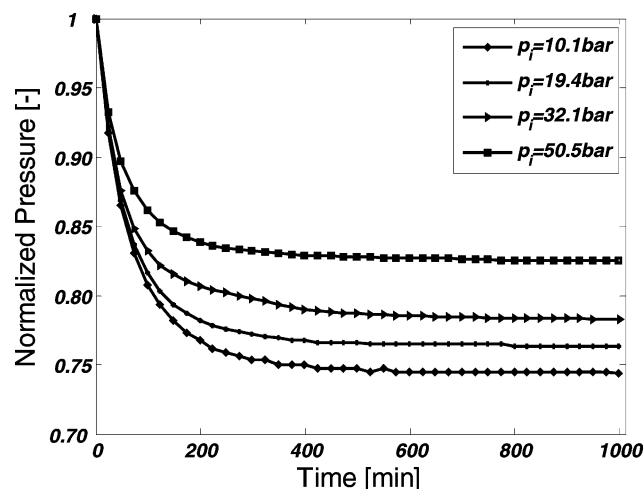


Figure 5. Pressure history of the experiments with different initial pressures. The pressure decline indicates the transfer of CO_2 into water. Initially the curves are steeper, showing the significance of natural convection.

the valve connecting the vessel containing the water was closed and the cell was isolated. This was the starting time of the experiment. The gas pressure was recorded every 100 s in a computer.

4. Results and Discussion

4.1. Experimental Observations. Figure 5 shows the history of the normalized CO_2 pressure of the experiments with different initial pressures. The gas pressure declines significantly at the initial stages of the experiment; i.e., it has a steep slope at the early times of the experiment. However, the slope of the curve becomes less steep with time, meaning that the mass-transfer rate decreases with time. The time needed for an overpressurized gas to reach equilibrium with the liquid below can be calculated using Fick's second law. However, in our experiments the measured mass-transfer rate over the interface turned out to be substantially larger than predicted using Fick's second law (see the dashed lines in Figures 11–14). An interpretation in terms of *two effective diffusion coefficients* has been presented in ref 9. The effective diffusion coefficient for the early stages of the experiments is 2 orders of magnitude higher than the molecular

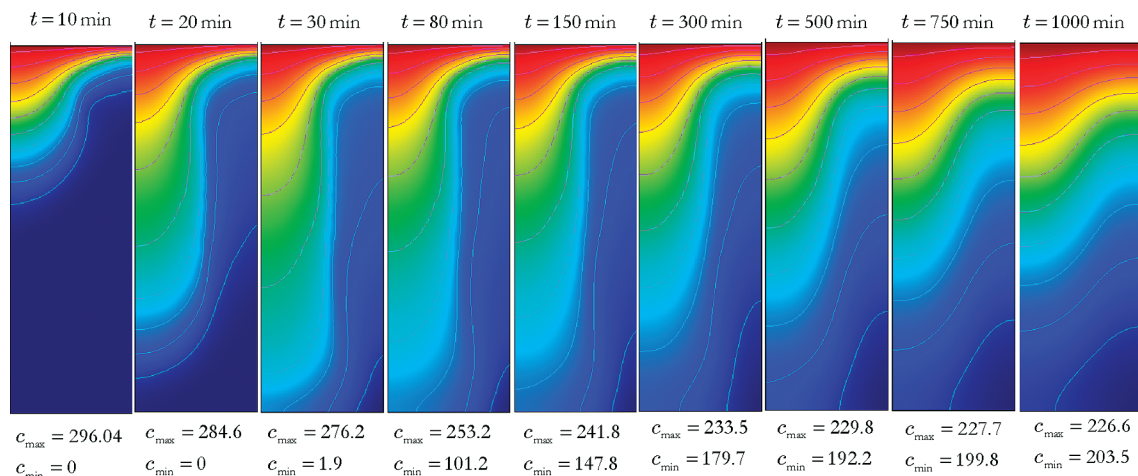


Figure 6. Evolution of CO₂ concentration profiles inside water with time at an initial pressure of $p_i = 10.1$ bar. The maximum (red) and minimum (blue) concentration values are different in each panel. The concentration values are expressed in mol/m³.

diffusivity of the CO₂ into water, indicating the presence of natural convection. Note that the effective diffusion coefficients are only a fitting parameter and have no physical meaning. The effect of natural convection increases as the initial pressure of the experiments increases. Nevertheless in all experiments the influence of the convection decreases as time elapses regardless of the initial pressure of the experiment.

4.2. CO₂ Concentration Inside the Liquid. The general trend of the concentration profiles for all experiments is similar, and therefore only the curves of the experiment with $p_i = 10.1$ bar will be presented. Nonetheless, the explanation holds for all experiments. Figure 6 shows the evolution of CO₂ concentration inside the water with time. The maximum and minimum concentrations are given below each image. These maximum (red) and minimum (blue) concentration values are different in each panel. This procedure allows using the full color span for displaying the results. When analyzing this profile, it is observed that as soon as CO₂ is put above the water, it starts to dissolve. The CO₂ concentration is higher near the center of the vessel. This increases the density of the liquid near the center, which induces an anticlockwise vortex in the vessel. The CO₂ concentration decreases at the interface (and near the interface) as the pressure in the gas chamber decreases while CO₂ is transferred far into the liquid. After about 30 min CO₂ reaches the bottom of the vessel. At this time the fluid has its maximum velocity (see Figure 7). With a simple scaling analysis it is possible to evaluate the significance of natural convection. The time scale for CO₂ diffusion through a water layer with thickness of $L_1 = 43$ mm at our experimental condition is $\sim L_1^2/D \approx 9.24 \times 10^5 \text{ s} \approx 256 \text{ h} \gg 30 \text{ min}$. As time elapses, the difference between the minimum and maximum values of the concentration becomes less; i.e., the distribution of CO₂ becomes more uniform in the liquid. This implies that convection effect dies out with time.

4.3. Velocity Profiles. Figure 7 presents the calculated vertical velocity, v_z , at different vertical positions as a function of the vessel radius for the experiment with the initial pressure of $p_i = 10.1$ bar. In accordance with the concentration profile, the flow is much faster in the center, obviously to ensure (water) mass conservation in a horizontal cross-section. In the entire volume of the vessel the ascending fluid flow has a low velocity close to the wall, where it approaches zero corresponding to the adherence of the fluid. The vertical velocity increases as fluid moves down in the region $43 < z < 33$ mm. From $z = 33$ mm downward the fluid starts to slow down again until it stops

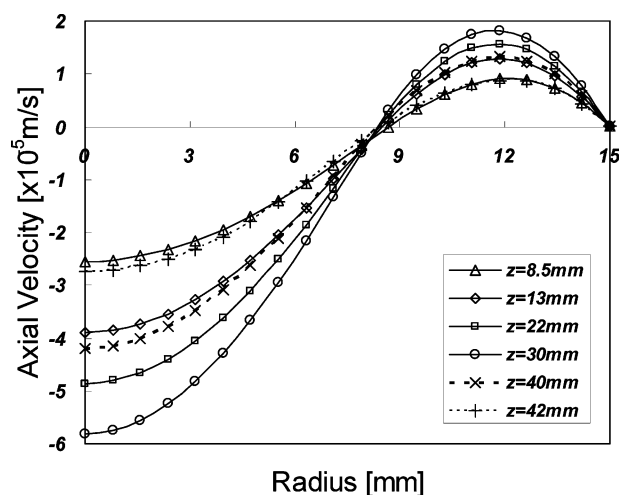


Figure 7. Axial velocity, v_z , at different positions at time $t = 60$ min for the experiment with an initial pressure of $p_i = 10.1$ bar.

at the bottom of the vessel ($z = 0$). In other words the flow is slower at the upper part close to the CO₂–water interface. A similar velocity pattern was numerically observed for a cylindrical cavity when its upper face was cooled by thermoelectrical Peltier effect following an exponential law.²⁶ It appears from the simulation results that at $z = 33$ mm there is no flow in the radial direction (see Figure 8). The radial velocity is 1 order of magnitude smaller than the vertical velocity, and it has different signs below and above $z = 33$ mm. This means that the vertical flow is mainly responsible for the enhancement of the transfer rate of CO₂ into water. The velocity change with time is shown in Figure 9 at a fixed position of $z = 30$ mm. Initially the liquid is at rest. When CO₂ is brought in contact with the liquid, it starts to move. The liquid velocity increases until the CO₂ front reaches the bottom of the vessel at $t \sim 30$ min. After that the fluid velocity decreases as more CO₂ is dissolved in the water with time. Note that at the end of our experiment the liquid velocity is very low but not zero. The fluid motion stops after about 3000 min when the water is fully saturated with CO₂. As can be seen from Figure 10, the liquid velocity increases as the initial pressure of the experiment (or the Rayleigh number) increases. Obviously, the relation is not linear. The pressure decline becomes faster as the Rayleigh number increases; i.e., the time to reach the equilibrium state for a constant volume of water decreases with increasing Rayleigh number, a result which can also be concluded from Figure 5.

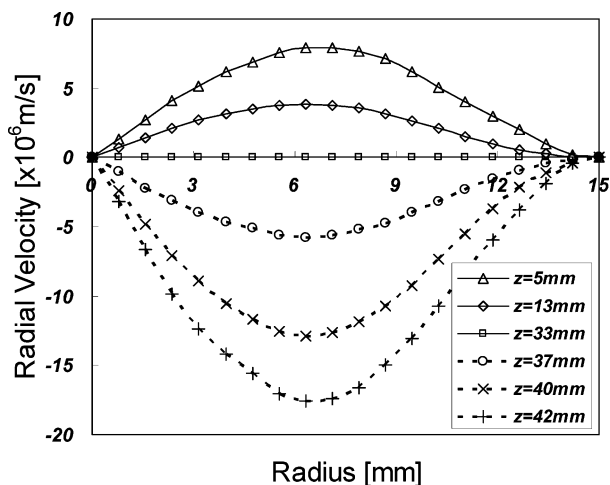


Figure 8. Radial velocity, v_r , at different positions at time $t = 60$ min for the experiment with an initial pressure of $p_i = 10.1$ bar.

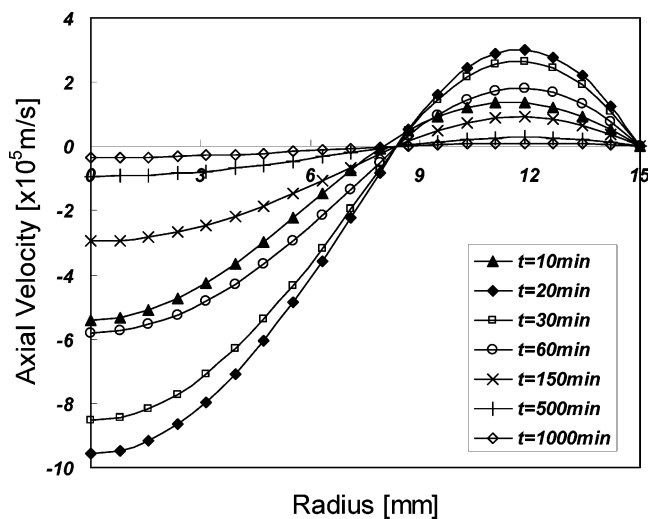


Figure 9. Axial velocity, v_z , at different times at $z = 30$ mm for the experiment with an initial pressure of $p_i = 10.1$ bar.

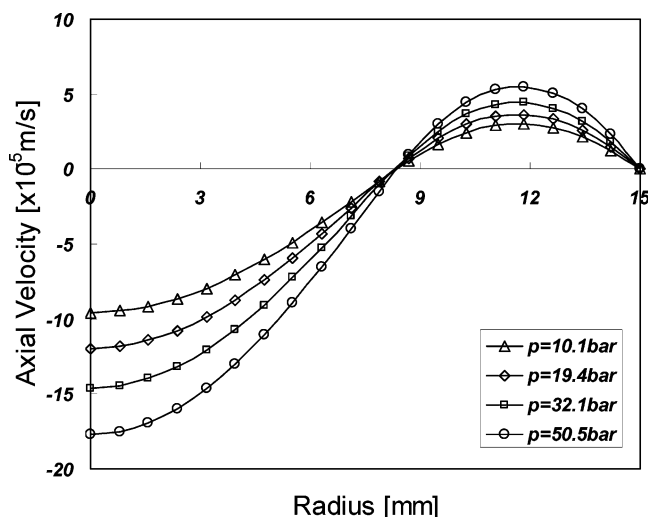


Figure 10. Calculated axial velocity, v_z , at $z = 30$ mm and $t = 20$ min for the experiments with different initial pressures.

4.4. Pressure Decline. As already mentioned CO_2 was injected from the storage vessel to the measurement vessel that was initially filled with water at atmospheric pressure. The sudden opening of the valve between the two vessels causes

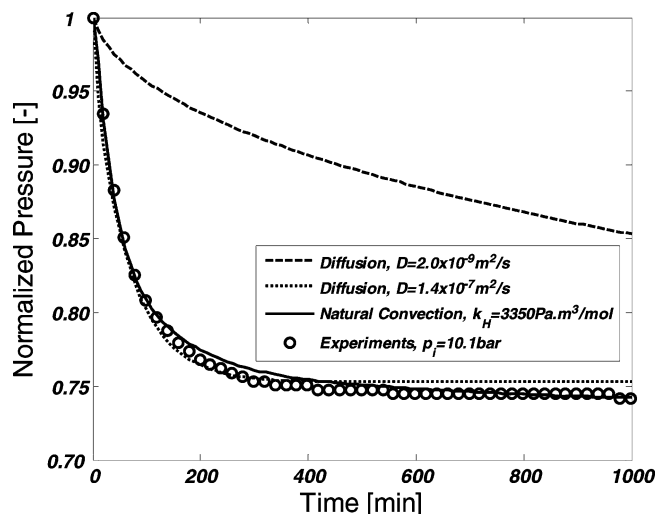


Figure 11. Comparison between the measured pressure data and the numerical model for $p_i = 10.1$ bar, $T = 30$ °C, $k_H = 3350$ Pa·m³/mol, and $D = 2.0 \times 10^{-9}$ m²/s. The dotted line is obtained with an effective diffusion coefficient of $D = 1.40 \times 10^{-7}$ m²/s, which is obtained from fitting the data to a Fickian diffusion model.

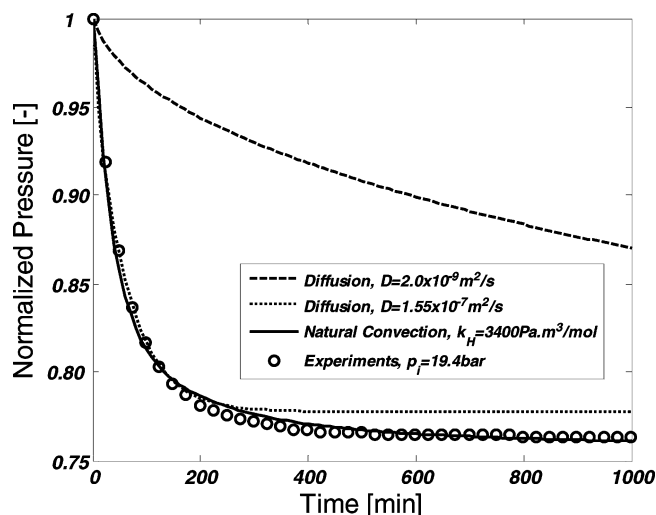


Figure 12. Comparison between the measured pressure data and the numerical model for $p_i = 19.4$ bar, $T = 30$ °C, $k_H = 3400$ Pa·m³/mol, and $D = 2.0 \times 10^{-9}$ m²/s. The dotted line is obtained with an effective diffusion coefficient of $D = 1.55 \times 10^{-7}$ m²/s.

disturbances, which may hamper a clear definition of the initial conditions. All the same adiabatic compression of CO_2 temporarily increases the temperature of the vessel.³⁶ As a result the system requires a short time to equilibrate. This effect is more significant at higher pressure as a larger mass of CO_2 is injected to the system. Our system measures pressures with 100 s intervals; therefore, we ignored the first two data points. This time is equivalent to the time at which CO_2 reaches equilibrium in the storage vessel (the pressure remains constant). In ref 8 the authors ignored the first 180 s of their experiments due to a similar effect.

Figures 11–14 plot the pressure history for the experiments with the initial pressures of $p_i = 10.1$, 19.4, 32.1, and 50.5 bar, respectively. These pressures are well below the critical pressure of CO_2 . The experimental data are compared with the theory described in section 2 with and without taking into account natural convection effects. In all cases the pressure decline rate is much larger than predicted by a Fickian diffusion process. For the computation values of β_c , k_H and Z_g are required. Note

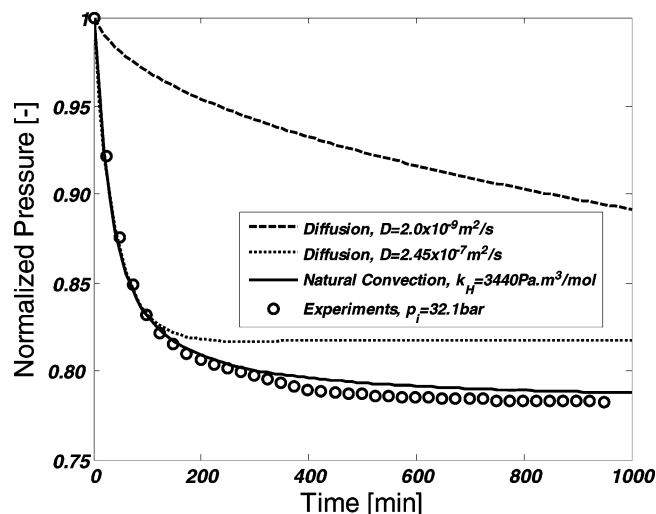


Figure 13. Comparison between the measured pressure data and the numerical model for $p_i = 32.1$ bar, $T = 30$ °C, $k_H = 3440$ Pa·m³/mol, and $D = 2.0 \times 10^{-9}$ m²/s. The dotted line is obtained with an effective diffusion coefficient of $D = 2.45 \times 10^{-7}$ m²/s.

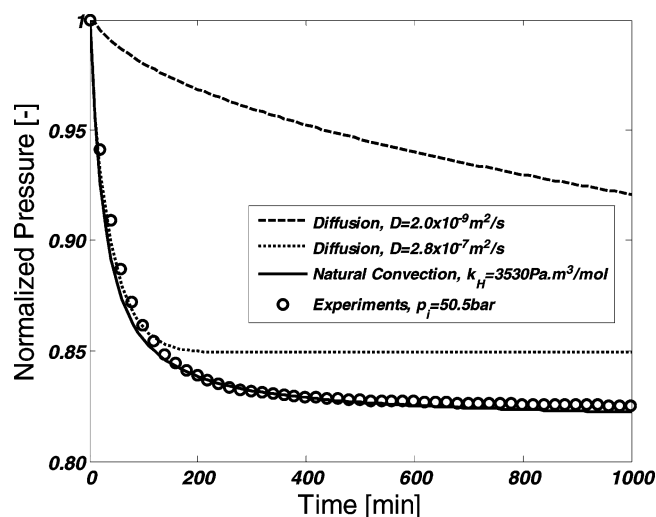


Figure 14. Comparison between the measured pressure data and the numerical model for $p_i = 50.5$ bar, $T = 30$ °C, $k_H = 3530$ Pa·m³/mol, and $D = 2.0 \times 10^{-9}$ m²/s. The dotted line is obtained with an effective diffusion coefficient of $D = 2.80 \times 10^{-7}$ m²/s.

that by choosing $\beta_c = 0$ in the simulation, diffusion will be the only transport mechanism and the results of the model agree well with the analytical solution obtained in ref 9. In the case of natural convection, the density differences are read from Figure 2 and then the concentration-dependent β_c is calculated for the conditions of each experiment using eq 1. Henry's coefficient, k_H , is obtained from Figure 3. The compressibility factor, Z_g , is calculated using the Span–Wagner equation of state (EoS)³⁷ for all pressures at the experimental temperature ($T = 30$ °C). For all of the experiments the match between the experimental data and the theory is within the experimental error (solid lines). To obtain the solid lines, the molecular diffusion coefficient of CO₂ ($D = 2.0 \times 10^{-9}$ m²/s) was used in the model. It is also possible to fit the experimental data by choosing *effective diffusion coefficients* and switching off the convection currents (dotted lines), similar to the models explained in refs 8 and 9. Such models are not physically justified, because comparing the values reported in ref 9 for $p_i = 10.1$ and 19.4 bar and the values obtained from our simulations reveal that the magnitude of the diffusion coefficient depends on the

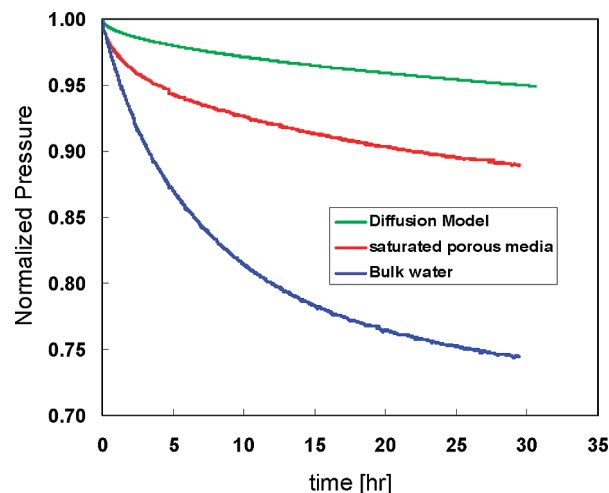


Figure 15. Comparison of the pressure history of the experiments with (red) and without porous media (blue). The experiments are done in a glass tube with radius of 3.5 mm at $p_i = 11$ bar.

geometry of the system (in this case radius and aspect ratio). Moreover, these models fail in accurately explaining the later stages of the experiments, because allowing an effective diffusion coefficient 2 orders of magnitude larger than molecular diffusivity of CO₂ results in equilibration times that are much shorter than the experiments (see Figures 11–14). In ref 8 the authors simulate experiments with duration of only 1 h. The extracted effective diffusion coefficients increase with increasing initial pressure, and they are in good agreement with the values reported in ref 8.

It should be mentioned that we also considered the possible contributions of Marangoni effect in our experiments. A rough calculation, based on a paper by Arendt et al.,¹⁶ shows that at our experimental conditions the mass-transfer coefficient due to natural (or free) convection is 1–2 orders of magnitude larger than the mass-transfer coefficient due to Marangoni convection. The reason could be that the interfacial tension between CO₂ and water does not change significantly at our experimental pressures, but it does change significantly from 1 to 100 bar. Strictly speaking at pressures above 10 MPa the IFT has asymptotic behavior.³⁸

Furthermore, in Figure 15 we plot the pressure history of two experiments in a glass tube with radius of 3.5 mm. In one experiment the glass tube is filled with only water,⁹ and in the other one the tube is filled with porous media of the same height and saturated with water.⁷ This figure shows that, although natural convection enhances the transfer rate in water-saturated porous media, its significance is less compared to bulk liquid. One has to remember that the critical time for the onset of natural convection is inversely proportional to the Rayleigh number.⁷ The Rayleigh number, Ra , appears in the flow equations of both cases, and therefore the rate of flow is an increasing function of Ra (see eqs 8 and 9 of ref 10 and eq 9 of ref 7). The equations of Ra imply that $(Ra)_{pm} \propto kL$ and $(Ra)_{bulk} \propto L^3$. In the comparison of the pressure behavior of the experiments with and without porous media the following points should be considered: First, the critical Ra for onset of convection in porous media is about 40, while for a clear fluid (or bulk liquid) convection occurs beyond a critical Ra of approximately 1700.³⁹ Second, from the Hagen–Poiseuille equation the permeability of the tube with radius of r_t is $k = r_t^2/8$, which gives the value of $k = 1.5 \times 10^6$ darcy for a tube with radius of 3.5 mm, whereas for porous medium the permeability is 1200 darcy, i.e., a factor of 1000 difference.

This can explain a factor of 10 difference in the transfer rates of the two systems presented in Figure 15. It should be also mentioned that the amount of water in porous media experiment is much less than bulk experiment and therefore the equilibrium pressures are different.

5. Conclusions

- We confirmed that mass-transfer rates can be measured in a relatively simple PVT cell, following the pressure history of the gas phase by extending our experimental database to a pressure range of 10–50 bar.

- A physical model based on density-driven natural convection and diffusion has been formulated. The model uses a number of simplifying assumptions, e.g., that Henry's law is applicable at the interface.

- The finite volume method (FVM) was used to solve the model equations numerically. The validity of the model was confirmed by comparing it to benchmark solutions. We used these results to validate a finite element model (FEM) using COMSOL. The advantage of using FEM is that local grid refinement is easier.

- According to the simulations the velocity increases until it reaches a maximum and then diminishes gradually as natural convection effect becomes less important. The maximum velocity corresponds to the time in which the CO₂ front reaches the bottom of the vessel.

- There is a strong correlation between the fluid velocity and the concentration profile with the experimental pressure decline rates. The pressure history obtained from the numerical model agrees well with the experimental data within experimental error. The matching does not use any fitting parameters.

Acknowledgment

This research was carried out as part of a project funded by Delft Earth Research. We thank the technicians of the Dietz laboratory of our faculty, especially H. van der Meulen and H. van Asten. We thank Prof. A. Firoozabadi and Dr. S. Rudolph for useful suggestions.

Nomenclature

a = empirical fitting parameter
 b = empirical fitting parameter
 c = concentration (mol/m³)
 c_p = heat capacity [(J/K)/m³]
 D = diffusion coefficient (m²/s)
 f = fugacity (Pa)
 g = acceleration due to gravity (m/s²)
 k_H = Henry's constant
 L = length of the tube (m)
 p = pressure (Pa)
 r = distance from center of the tube (m)
 R = radius of the tube (m)
 Ra = Rayleigh number
 T = temperature (K, °C)
 t = time (s)
 v = velocity (m/s)
 z = distance from the bottom of the tube (m)
 Z_g = gas compressibility factor

Greek Letters

ρ = density of the fluid (kg/m³)
 β_c = volumetric expansion coefficient (m³/mol)

α = empirical fitting parameter
 μ = viscosity of the fluid (kg·m/s)
 ν = kinematic viscosity (m²/s)

Subscripts

0 = reference value of the quantity
 g = gas
 i = initial value
 w = water
 r = quantity in r -direction
 z = quantity in z -direction

Literature Cited

- (1) Metz, B.; Davidson, O.; de Coninck, H.; Loos, M.; Meyer, L., Eds. *IPCC Special Report on Carbon Dioxide Capture and Storage*; Cambridge University Press: Cambridge, U.K., 2005.
- (2) Pruess, K.; Garcia, J. Multiphase Flow Dynamics during CO₂ Disposal into Saline Aquifers. *Environ. Geol.* **2002**, *42*, 282.
- (3) Bruant, R. G.; Guswa, A. J.; Celia, M. A.; Peters, C. A. Safe Storage of CO₂ in Deep Saline Aquifers. *Environ. Sci. Technol.* **2002**, *36*, 240A.
- (4) Naderi Beni, A.; Kühn, M.; Meyer, R.; Clauser, C. Geological Sequestration of CO₂ in North Rhine Westphalia (Germany). *Proceedings of the Sino-German Workshop*, Goslar, Germany, Sep 17–20, 2007.
- (5) Gmelin, L. in *Gmelin Handbuch der anorganischen Chemie*, 8; Auflage. Kohlenstoff, Teil C3, Verbindungen; 1973; ISBN 3-527-81419-1.
- (6) Lindeberg, E.; Wessel-Berg, D. Vertical Convection in an Aquifer Column under a Gas Cap of CO₂. *Energy Convers. Manage.* **1997**, *38*, S229.
- (7) Farajzadeh, R.; Salimi, H.; Zitha, P. L. J.; Bruining, J. Numerical Simulation of Density-Driven Natural Convection with Application for CO₂ Injection Projects. *Int. J. Heat Mass Transfer* **2007**, *50*, 5054.
- (8) Yang, C.; Gu, Y. Accelerated Mass Transfer of CO₂ in Reservoir Brine Due to Density-Driven Natural Convection at High Pressures and Elevated Temperatures. *Ind. Eng. Chem. Res.* **2006**, *45*, 2430.
- (9) Farajzadeh, R.; Barati, A.; Delil, H. A.; Bruining, J.; Zitha, P. L. J. Mass Transfer of CO₂ into Water and Surfactant Solutions. *Pet. Sci. Technol.* **2007**, *25* (12), 1493.
- (10) Farajzadeh, R.; Delil, H. A.; Zitha, P. L. J.; Bruining, J. *Enhanced Mass Transfer of CO₂ into Water and Oil by Natural Convection*, SPE 107380, SPE Europec/EAGE Annual Conference and Exhibition, London, U.K., Jun 11–14, 2007.
- (11) Weir, G. J.; White, S. P.; Kissling, W. M. Reservoir Storage and Containment of Greenhouse Gases. *Energy Convers. Manage.* **1995**, *36* (6–9), 531.
- (12) Riazi, M. R. A New Method for Experimental Measurement of Diffusion Coefficients in Reservoir Fluids. *J. Pet. Sci. Eng.* **1996**, *14* (3–4), 235.
- (13) Denoyelle, L.; Bardon, C. *Diffusivity of Carbon Dioxide into Reservoir Fluids*, CIM Annual Genral Meeting (paper 114), Ottawa, Canada, Apr. 15–19, 1984.
- (14) Renner, T. A. Measurement and Correlation of Diffusion Coefficients for CO₂ and Rich-Gas Applications. *SPE Reservoir Eng.* **1988**, *3* (2), 517.
- (15) Wang, L. S.; Lang, Z. X.; Guo, T. M. Measurement and Correlation of the Diffusion Coefficients of Carbon Dioxide in Liquid Hydrocarbons under Elevated Pressures. *Fluid Phase Equilib.* **1996**, *117*, 364.
- (16) Arendt, B.; Dittmar, D.; Eggers, R. Interaction of Interfacial Convection and Mass Transfer Effects in the System CO₂-Water. *Int. J. Heat Mass Transfer* **2004**, *47* (17–18), 3649.
- (17) Ashcroft, S.; Ben Isa, M. Effect of Dissolved Gases on the Densities of Hydrocarbons. *J. Chem. Eng. Data* **1997**, *42*, 1244.
- (18) Ennis-King, J.; Paterson, L. Role of Convective Mixing in the Long-Term Storage of Carbon Dioxide in Deep Saline Aquifers. *SPE J.* **2005**, *10* (3), 349.
- (19) Riaz, A.; Hesse, M.; Tchelepi, A.; Orr, F. M. Onset of Convection in a Gravitationally Unstable Diffusive Boundary Layer in Porous Medium. *J. Fluid Mech.* **2006**, *548*, 87.
- (20) Vella, D.; Huppert, H. E. Gravity Currents in a Porous Medium at an Inclined Plane. *J. Fluid. Mech.* **2006**, *555*, 333.
- (21) Farajzadeh, R.; Farshbaf Zinati, F.; Zitha, P. L. J.; Bruining, J. Density Driven Natural Convection in Layered and Anisotropic Porous Media. *Proceedings of the 11th European Conference on Mathematics in Oil Recovery (ECMOR X1)*, Bergen, Norway, Sep. 8–11, 2008.
- (22) Bird, R. B.; Stewart, W. E.; Lightfoot, E. N. *Transport Phenomena*, 2nd rev. ed.; Wiley: New York, 2007.

- (23) Landau, L. D.; Lifshitz, E. M. *Fluid Mechanics*, Vol. 6 of course of theoretical physics (translated from Russian by Sykes J. B., Reid W. H.), 4th ed.; Pergamon Press: New York, 1975; pp 212–218.
- (24) Güçeri, S.; Farouk, B. Numerical Solutions in Laminar and Turbulent Natural Convection; In *Natural Convection, Fundamentals and Applications*; Kakac, S.; Aung, W.; Viskanta, R.; Hemisphere: Bristol, PA, 1985; pp 615–655.
- (25) Patankar, S. V. *Numerical Heat Transfer and Fluid Flow*; Hemisphere: New York, 1980.
- (26) Bairi, A. Transient Natural 2D Convection in a Cylindrical Cavity with the Upper Face Cooled by Thermoelectric Peltier Effect Following an Exponential Law. *Appl. Thermal Eng.* **2003**, 23, 431.
- (27) Becker, B. R.; Drake, J. B. Finite Element Simulation of Viscous Incompressible Flows. *Math. Modell.* **1987**, 8, 245.
- (28) Ferreira, S. Transient Natural Convection Cooling of a Vertical Circular Cylinder. *Nucl. Eng. Des.* **1974**, 31, 346.
- (29) Ramaswamy, B. Solution of the Boussinesq Equations by the Finite Element Method. *Finite Elem. Anal. Des.* **1989**, 6, 319.
- (30) Greenwood, N. N.; Earnshaw, A. *Chemistry of the Elements*, 2nd ed.; Butterworth Heinemann: Oxford, U.K., 1997.
- (31) Tegetmeier, A.; Dittmar, D.; Fredenhagen, A.; Eggers, R. Density and Volume of Water and Triglyceride Mixtures in Contact with Carbon Dioxide. *Chem. Eng. Process.* **2000**, 39, 399.
- (32) Akinfiev, N. N.; Diamond, L. W. Thermodynamic Description of Aqueous Nonelectrolytes at Infinite Dilution over a Wide Range of State Parameters. *Geochim. Cosmochim. Acta* **2003**, 67, 613.
- (33) Diamond, L. W.; Akinfiev, N. N. Solubility of CO₂ in Water from –1.5 to 100 °C and from 0.1 to 100 MPa: Evaluation of Literature Data and Thermodynamic Modeling. *Fluid Phase Equilib.* **2003**, 208, 265.
- (34) Fogg, P. G. T.; Gerrard, W. *Solubility of Gases in Liquids*; Wiley: New York, 1991; pp 281–314.
- (35) Gertz, Kh.; Loeschcke, Hh. Determination of Diffusion Coefficient of CO₂ in the Water with a Conic Tube. *Helv. Physiol. Pharmacol. Acta* **1954**, 12 (4), 72.
- (36) Edmister, W. C.; Lee, B. I. *Applied Hydrocarbon Thermodynamics*, 2nd ed.; Gulf: Houston, TX, 1984; Vol. 1.
- (37) Span, R.; Wagner, W. A New Equation of State for Carbon Dioxide Covering the Fluid Region from the Triple-Point Temperature to 1100 K at Pressures up to 800 MPa. *J. Phys. Chem. Ref. Data* **1996**, 25, 1509.
- (38) Chiquet, P.; Daridon, J.-L.; Broseta, D.; Thibeau, S. CO₂/Water Interfacial Tensions under Pressure and Temperature Conditions of CO₂ Geological Storage. *Energy Convers. Manage.* **2007**, 48, 736.
- (39) Ozoe, H.; Takemoto, M.; Churchill, S. W. Finite-Element Analysis of Laminar Natural Convection in Confined Rectangular Regimes-Extrapolation to Zero Element Size. *Numer. Heat Transfer, Part B* **1986**, 9 (3), 323.

Received for review October 8, 2008

Revised manuscript received May 15, 2009

Accepted May 15, 2009

IE801521U